USGS

Seismic Imaging Evidence For Faulting Across The Northwestern Projection of the Silver Creek Fault, San Jose, California

by

R. D. Catchings, M. R. Goldman, C. Gandhok, M. J. Rymer, and D. H. Underwood

Open-File Report 00-325

2000

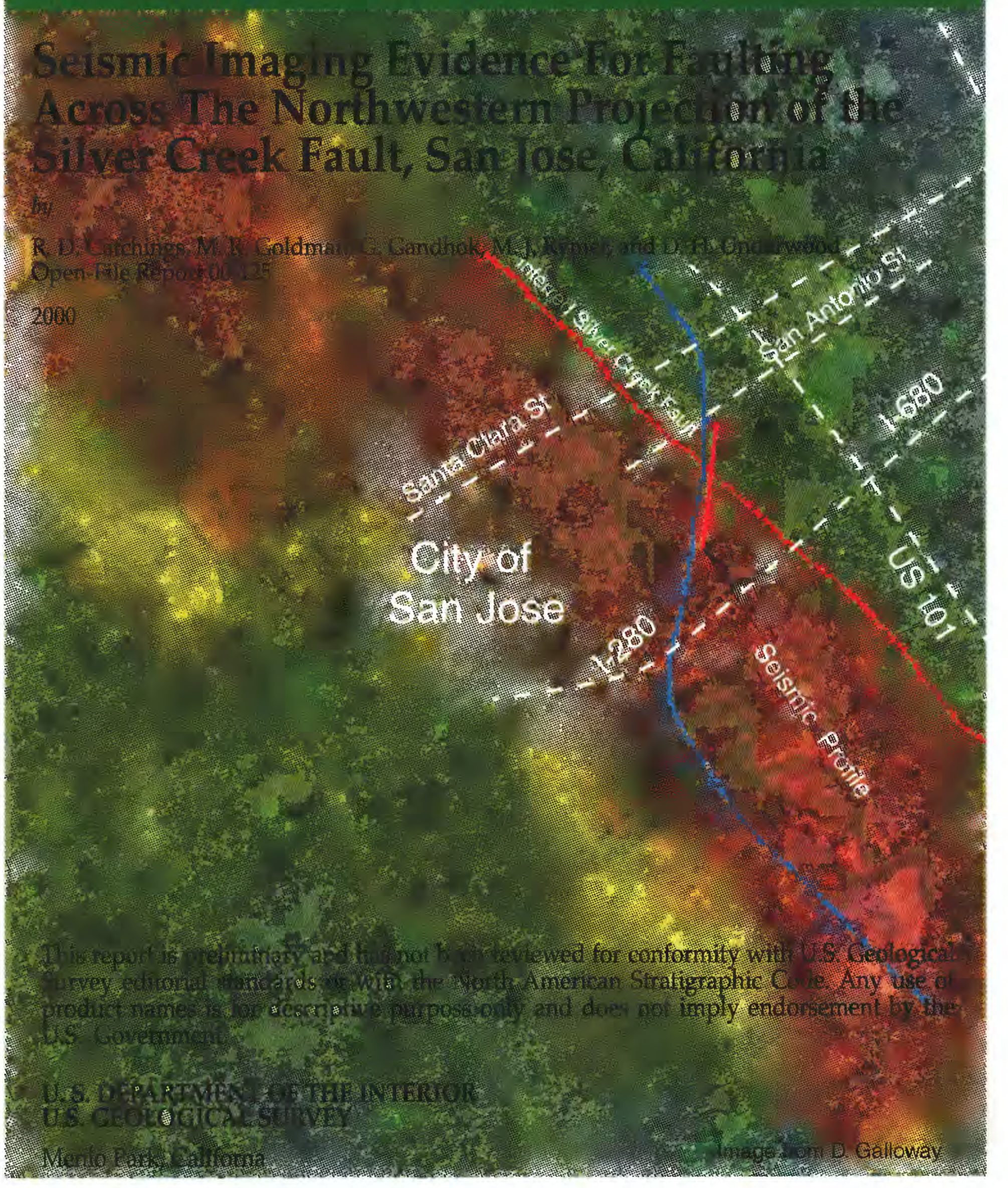

U.S. DEPARTMENT OF THE INTERIOR
U.S. GEOLOGICAL SURVEY

Menlo Park, California

Image from D. Galloway

Table of Contents

List of Tables

List of Figures

Introduction

In this report, we present acquisition parameters, data, and an interpretation of a seismic imaging test that was conducted in the central part of the city of San Jose, California, within the central Santa Clara Valley (Fig. 1a). The principal objectives of the seismic imaging survey were to: (1) look for evidence of shallow-depth faulting, (2) laterally image subsurface stratigraphic units, (3) measure seismic velocities in the shallow subsurface, and (4) test acquisition parameters needed to successfully conduct high-resolution seismic imaging surveys in the San Jose area. The seismic data from this test survey is used to address issues related to both seismic hazards and groundwater resource.

The large population and lifelines within the Santa Clara Valley, combined with the possibility of concealed and potentially active faults directly beneath highly urbanized areas, present a high potential for earthquake hazards. On the basis of geologic evidence, Bortugno et al. (1991) suggest that there may be a number of Quaternary faults beneath surficial sediments of the Santa Clara Valley; however, most of the Santa Clara Valley is covered at the surface by Quaternary sediments (Wagner et al., 1991; Wentworth et al., 1999) or cultural features that make it difficult to locate or confirm the existence of these faults. Bortugno et al. (1991) suggest that the most recent movement on many of the faults beneath the Santa Clara Valley is not known but may be Holocene or Historic. Of particular concern to this study is the Silver Creek fault, which is exposed in outcrop in hills about 5 km to the southeast of the immediate study area, and is assumed to be between 55 and 70 km in length (Bortugno et al., 1991; Wagner et al, 1991). It is not certain that the Silver Creek fault extends northwestward beneath the sediments of the Santa Clara Valley as mapped. Furthermore, if the Silver Creek fault does extend beneath the Santa Clara Valley as mapped, the age of it's most recent movement is not known. Knowledge of fault locations, their lengths (which influence maximum magnitude), and their most recent movement are three of the parameters needed to estimated potential seismic hazards in the Santa Clara Valley.

The Silver Creek and other faults within the Santa Clara Valley may segment groundwater within the Santa Clara Valley. Interferometric Synthetic Aperture Radar (INSAR) images (Fig. 1b) show evidence of uplift corresponding to the northwestern side of the geologically inferred (Bortugno et al., 1991) Silver Creek fault. If the apparent area of uplift identified on the INSAR image results from movement or stratigraphic changes attributable to the Silver Creek fault, the Silver Creek fault may form a groundwater barrier.

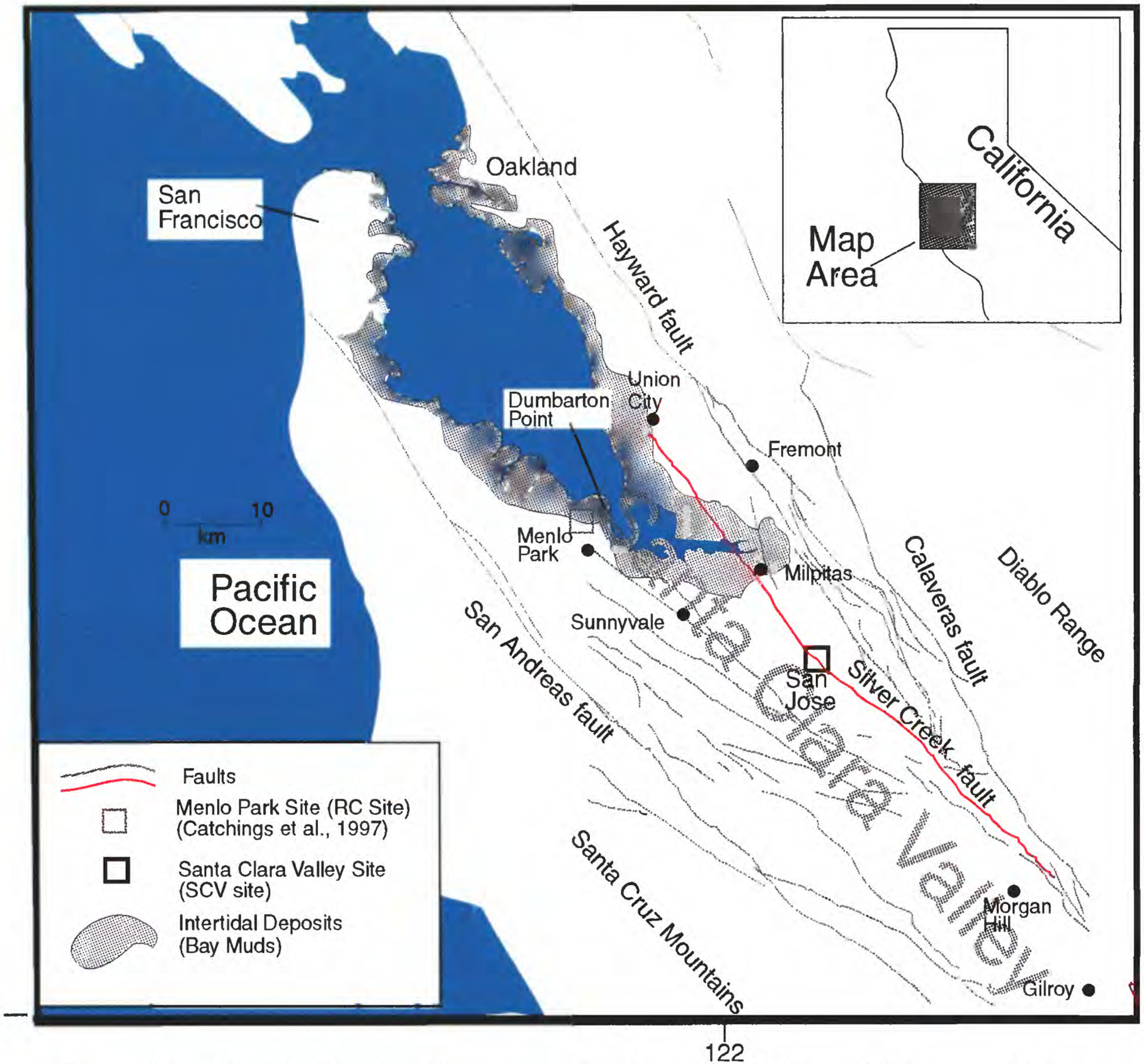

Fig. 1a Map of the San Francisco Bay area and the Santa Clara Valley with Quaternary faults (from Bortugno et al., 1991) and the locations of study areas. The Silver Creek fault is shown in red.

Santa Clara Valley Seismic Profile and INSAR Image Along Inferred Silver Creek Fault

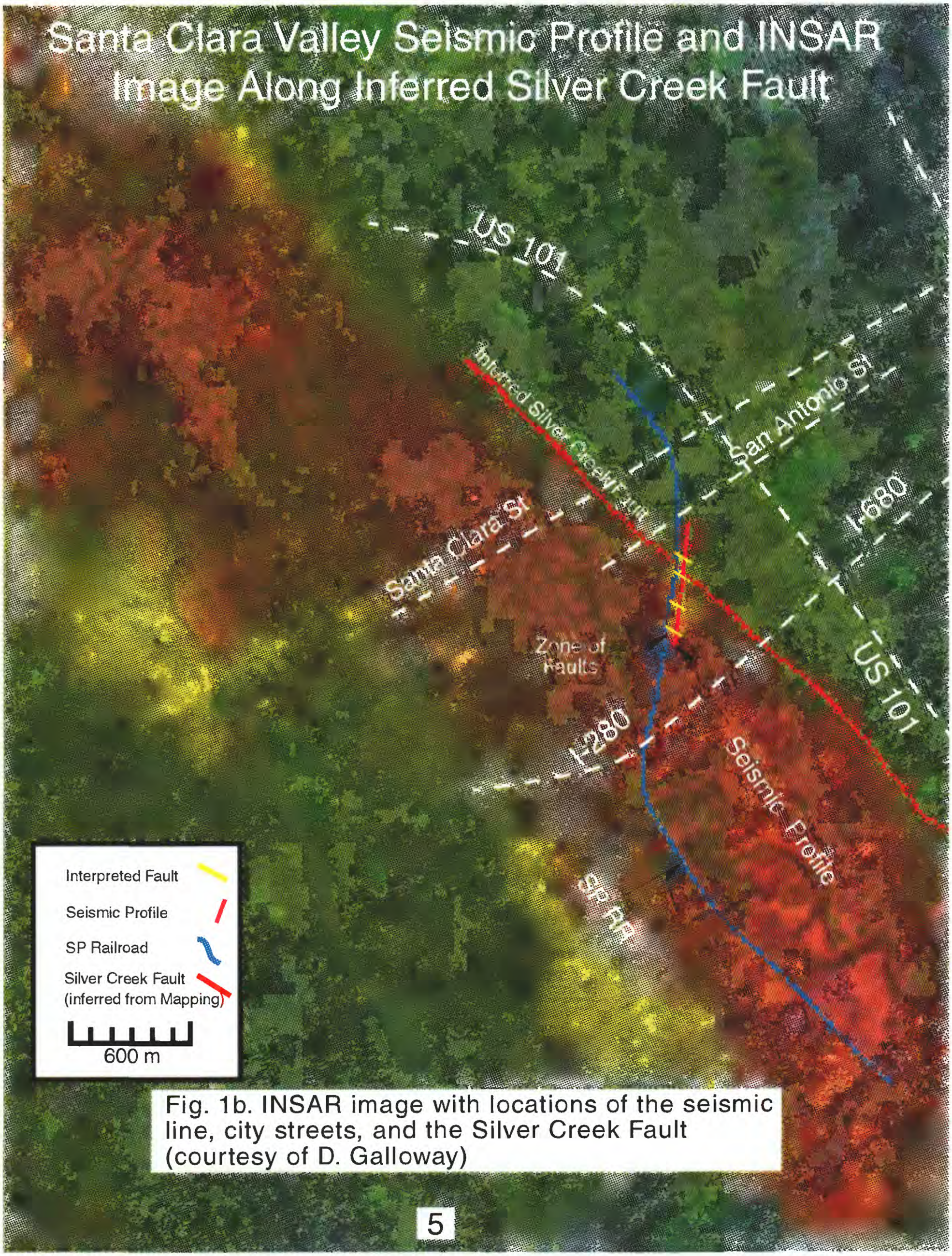

Fig. 1b. INSAR image with locations of the seismic line, city streets, and the Silver Creek Fault (courtesy of D. Galloway)

Storage and recovery of groundwater resources would be affected by the presence of such a barrier.

High-resolution seismic imaging within the Santa Clara Valley, combined with other geoscientific studies, can potentially resolve some of the unknown issues related to location, length, recency of movement of faults and stratigraphic configurations related to groundwater resources.

Local Geology and Tectonics

The city of San Jose lies within a 5- to 20-km-wide valley, known as the Santa Clara Valley. The Santa Clara Valley is bound on the east by the Diablo Range and on the west by the Santa Cruz mountains (Fig. 1a). To the north, the Santa Clara Valley includes parts of the southern San Francisco Bay and to the south, it attenuates near the convergence of the Calaveras and San Andreas faults. The surface geology of the Santa Clara Valley consists largely of Quaternary (Holocene and Pleistocene) sediments, but there are local hills within the valley with surficial Mesozoic ultramafics and Jurassic sandstones and limestones (Wagner et al., 1991). Numerous faults have been inferred or mapped within or adjacent to the Santa Clara Valley, including the Hayward, the San Andreas, the Calavaras, the Monte Vista, and unnamed faults (Bortugno et al., 1991). These faults are predominantly strike-slip, but may include local thrust, reverse, normal, and wrench faults. The most recent movement on many of the faults is known to be historic, but most are at least Late Quaternary or Holocene (Bortugno et al., 1991).

Within the immediate study area, the surficial sediments are Holocene, except where they have been replaced by man-made materials. Older Plio-Pleistocene non-marine sand and gravel, Tertiary marine sedimentary rocks, and Franciscian Complex rocks are believed to underlie the surficial sediments (Wagner et al., 1991). Faulting within the immediate study area is poorly determined due to the surficial Quaternary sediments. The Silver Creek fault is believed to trend through the study area, extending northwestward to Union City and southeastward to Morgan Hill (Bortugno et al., 1991). Movement on the Silver Creek fault, where it is exposed about 5 km southwest of the immediate study area, is known to be Quaternary in age, with possible historic movement (Bortugno et al., 1991).

Seismic Survey

An approximately 620-m-long seismic reflection/refraction survey was conducted in the city of San Jose in July 1999 by the US Geological Survey's High-Resolution Seismic Imaging Group. The profile trended NE-SW along a stretch of the Western Pacific Railroad, west of U. S. Highway 101 between San Antonio street and Interstate 280 (Fig. 1b). The seismic profile originated about 50 m southeast of E. San Antonio street and crossed four streets, including McLaughlin avenue, North 24 th street, South 23rd street, and William street. The Western Pacific railway site was chosen because it provided a linear swath through the city that was free of buildings and other cultural features and because it crossed the geologically and geophysically inferred northern extension of the Silver Creek fault.

Approximately 3 seconds of data were recorded on two Geometrics Strataview RX ™ seismographs, each with 60 active channels. The data were stored on the hard drive of the Geometrics Strataview computers during field acquisition and were later downloaded to 4-mm tape for permanent storage in SEG-Y format.

Sensors consisted of 120 40-Hz, single-element, Mark Products L-40A™ geophones spaced at 5 m along the profile. Seismic sources (shots), located at a depth of about 0.3 m, were generated by a BETSY Seisgun™ using 8-gauge shotgun blanks. Shots were spaced at 5 m increments along the profile and were co-located (1 m lateral offset) with the geophones. Shot timing was determined electronically at the seismic source when a hammer, used to trigger the seisgun, electrically closed contact with the Betsy Seisgun, sending an electrical signal to the seismograph.

Table 1. Acquisition parameters for Santa Clara Valley seismic profile. Distance is relative to the first shot point.

Profile #	Orientation	Length of geophone Profile (m)	Length of shot Point Profile (m)	No. of shots	No. of CDPs	Maximum fold
Profile 1	NE-SW	564.5	619.6	109	238	95

Data Acquisition

In seismic sections, artifacts that are mistaken for structure can result from geophones or shots locations with significant elevation variations if those elevation variations are not accounted for in processing the data. Deviations from a linear array of

geophones or shots can also create artifacts in the data. To properly account for the variations in geometry, each shot point and geophone location was surveyed using an electronic distance meter with theoretical accuracies of a few centimeters. Geophone locations along the profile varied by less than 1.5 m over a distance of about 600 m (Fig. 2), resulting in little need for elevation statics. The alignment of geophones varied from a straight line by about 3 m at two locations along the 600-m-long line (Fig. 3). These 3-m misalignments were necessary to maintain a continuous array across McLaughlin avenue and South 23rd street. A minor variation (0.5 m) in the linear array of geophones also occurred near William street.

Variations in shot point elevation (Fig. 4) and linearity of shot points (Fig. 5) are similar to those of the geophones. The shot array, however, is longer than the geophone array because we attempted to increase the fold at the ends of the geophone array. Shot points locations within the city streets (McLaughlin, S. 23rd, and William) were not used. There were two shots beyond the northeastern end of the profile and 11 shots beyond the southwestern end of the seismic line. A total of 16 shot point locations were not used along the profile due to cultural features.

Fold (the theoretical number of times a reflection occurs at a given subsurface location) along the Santa Clara Valley line was smoothly varying because of the stationary recording array (Fig. 6). Maximum fold of about 95 was obtained in the center of the seismic profile and decreased to about 1 at the ends of the profile. Because maximum folds were in the middle of the seismic profile, the most reliable reflection images for the deeper structure should theoretically be near the center of the profile. However, due to poor coupling between the source and the Earth and due to higher cultural noise near the center of the profile, our most reliable image below about 100 m depth may be near the ends of the profiles.

Seismic Data Processing

Both reflection and refraction data were acquired simultaneously by using a shoot-through configuration, whereby shots are systematically fired through the recording array. This type of data acquisition has numerous advantages over conventional seismic data acquisition methods because detailed velocity data are available and maximum folds (redundancy of reflection data points) are typically greater.

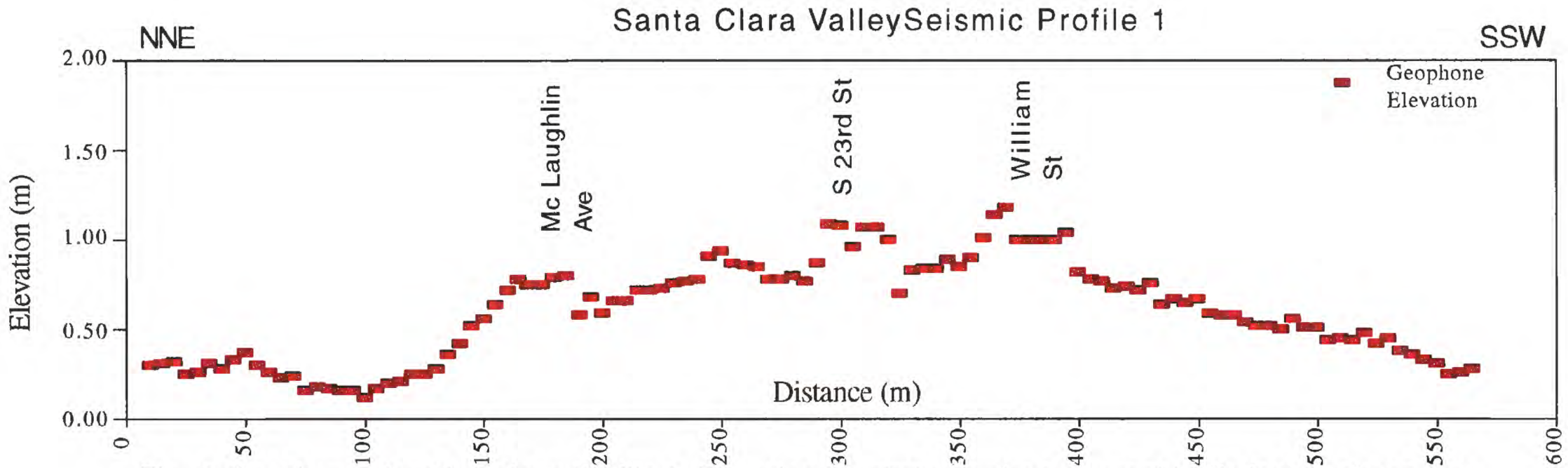

Fig. 2. Geophone elevation along Profile 1. Elevation is relative to the topographically lowest shot point along the profile. Crossing streets are labeled.

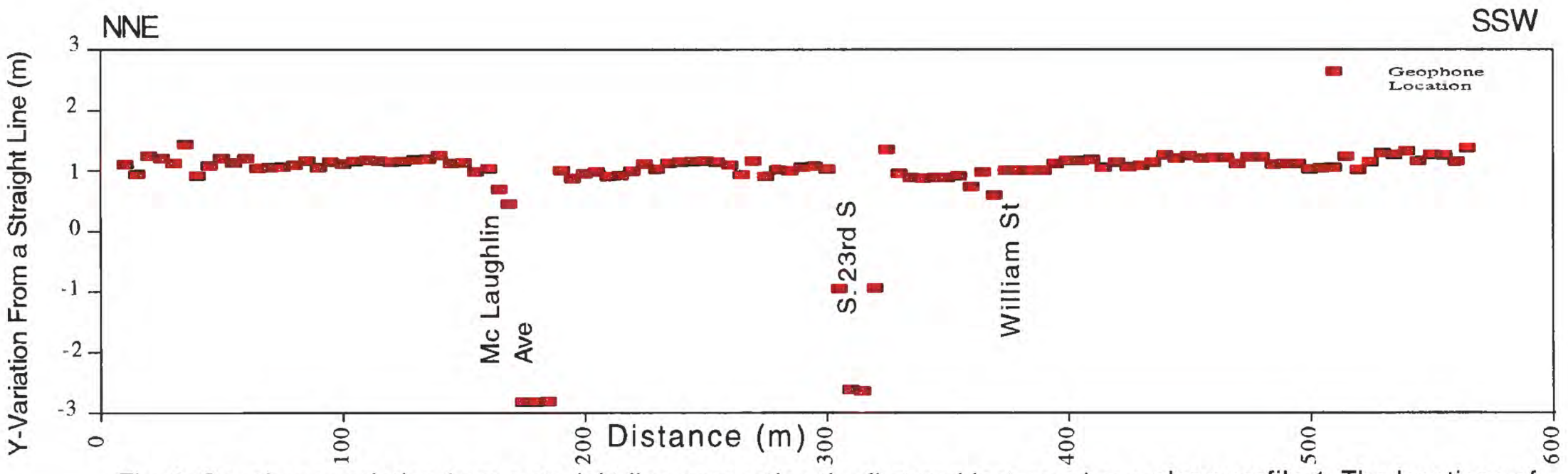

Fig. 3. Geophone variation from a straight line connecting the first and last geophone along profile 1. The locations of crossing streets are labeled.

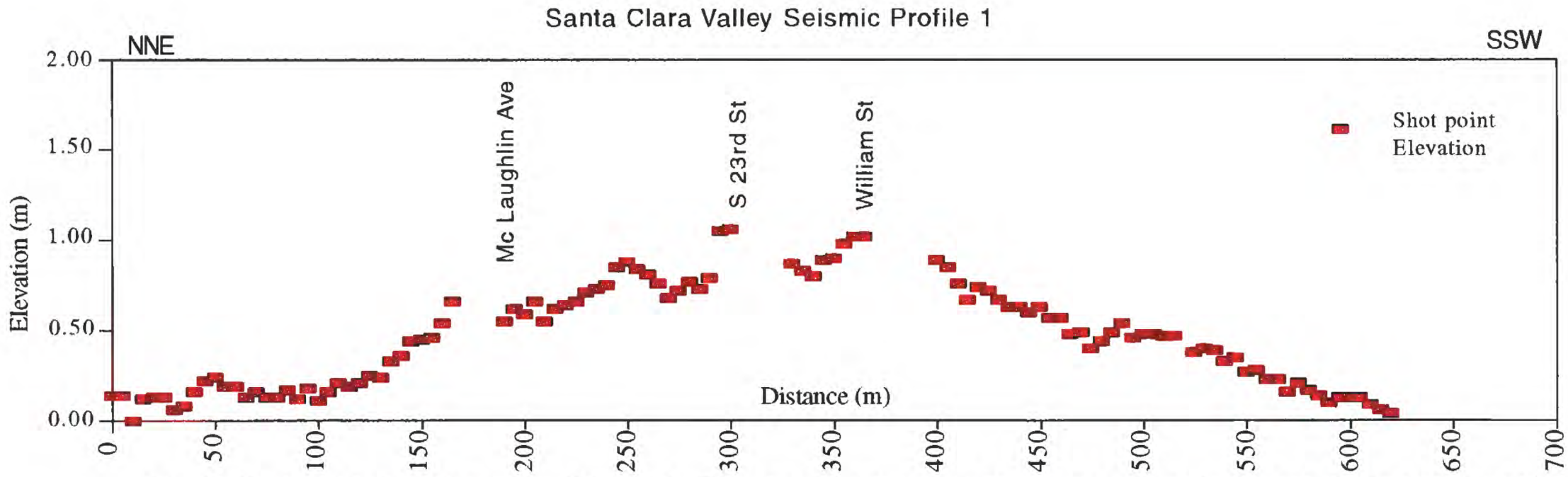

Fig. 4 Shot point elevation along Profile 1. Elevation is relative to the topographically lowest shot pont along the seismic profile. The location of crossing streets are labeled.

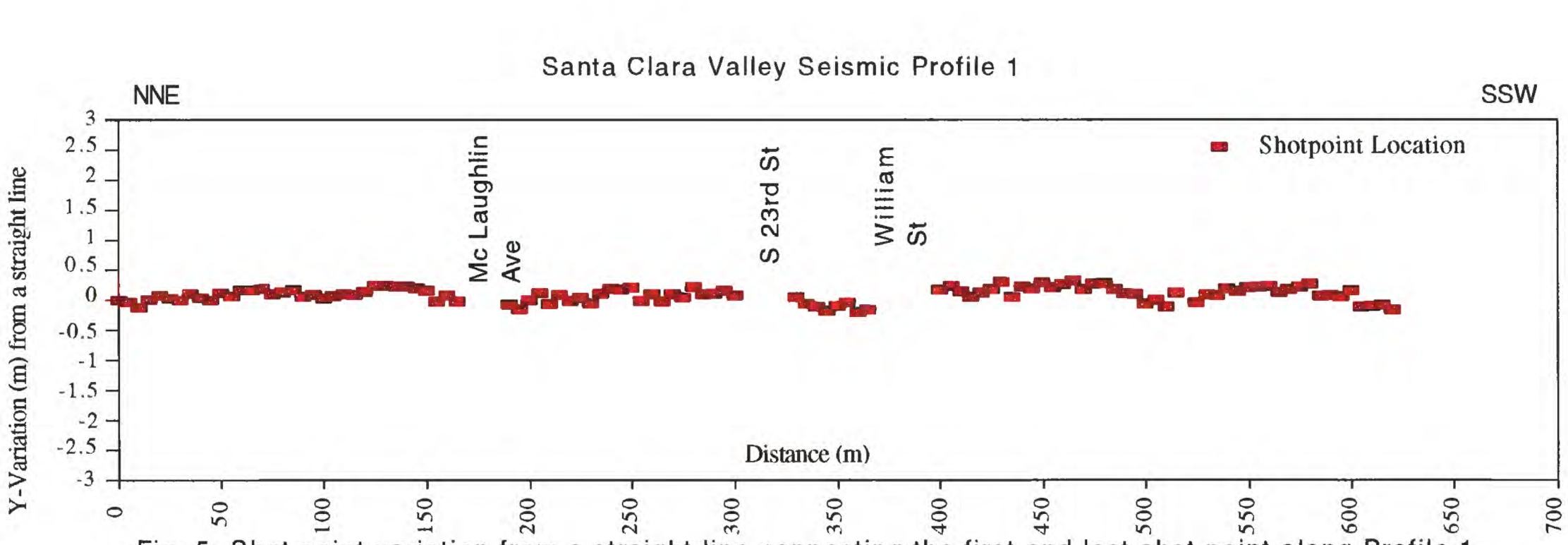

Fig. 5. Shot point variation from a straight line connecting the first and last shot point along Profile 1. Locations of cross streets are labeled.

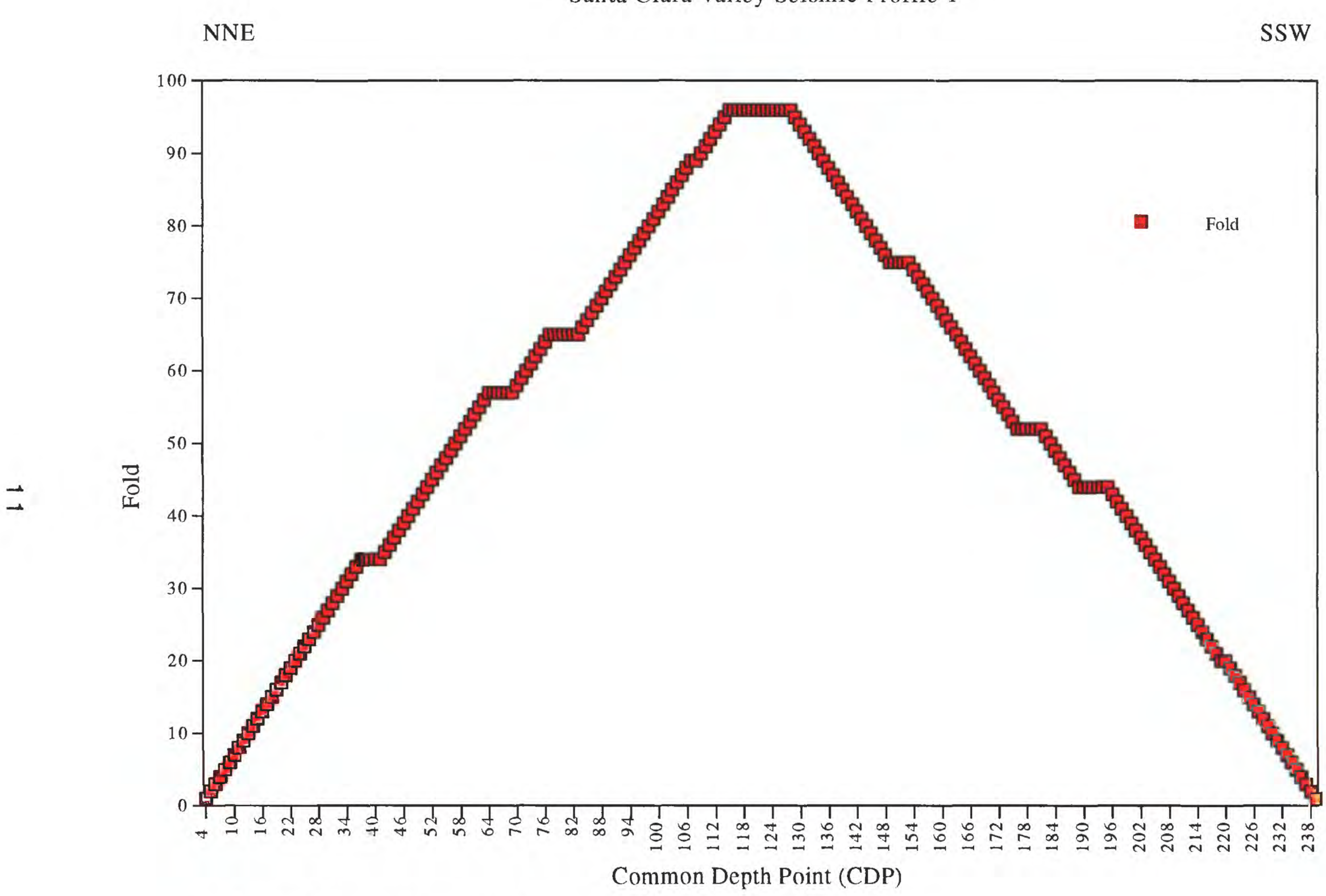

Fig. 6. Fold as a function of common depth points along Profile 1.

Seismic Refraction Velocity Analysis

We used two methods of seismic data processing, refraction analysis and reflection processing. In the refraction data processing, we used a seismic tomographic inversion method developed by Hole (1992), whereby, first arrivals on each seismic trace were used to measure velocities at depths ranging from about 3 m below the surface to about 30 m. For greater depths, velocities needed for seismic reflection stacking were determined using semblence and parabolic methods and apriori knowledge of the local geology derived from a seismic profile in nearby Menlo Park (Fig. 1a). We used the velocities derived from these methods to convert the reflection time-images to depth-images and to migrate the seismic reflection images.

Seismic Reflection Processing

Seismic reflection data processing was accomplished on a Sun Sparc 20 ™ computer using an interactive seismic processing package known as PROMAX™. The following steps were involved in data processing:

Geometry Installation

Lateral distances and elevations described above were used to define the geometrical set up of each profile. We installed the electronically-measured geometries into the ProMAX™ processing package for each profile separately so that shot and receiver elevations and locations could be accounted for in the processing routine.

Trace Editing

Occasionally, bad coupling between the geophones and the ground, malfunctioning geophones, or cultural noise close to the seismic receivers resulted in unusually noisy traces at those locations. Traces representing those locations were edited. However, such traces were not always unsuitable for each shot gather; therefore, independent trace editing was employed for each shot gather.

Bandpass Filtering

Most of the data of interest for seismic imaging and velocity measurement are between 25 and 200 Hz, and most of the undesirable seismic data, such as surface waves and shear waves, were below about 35 Hz. We used a final bandpass filter with a low cut of 30 Hz to remove most surface and shear waves as well as cultural noise.

F-K Filtering

Not all surface waves were removed by simple bandpass filtering. To remove those surface waves and air waves that were not removed by bandpass filtering, we used a FK filter.

Timing Corrections

Although the shotgun source electronically triggers the seismographs, there are small (~2 ms) delays between the electrical trigger and the actual shotgun explosions. We corrected for the delays by removing a constant 2 ms from the start time of each shotgather.

Velocity Analysis

Velocities in the shallow section (~1 m to ~150 m) were determined using velocity inversion techniques, but velocities in the deeper section were determined using shotgathers and CDP stacks.

Elevation Statics

Elevation statics were also employed to correct for variations in elevations using the electronically-determined locations and velocities that were derived from the refraction velocity analysis.

Moveout Correction

Due to progressively greater traveltimes for the seismic waves to reach sensors that were progressively farther from each shot point, there was a delay (moveout) for each seismic arrival on the seismic record. To sum (stack) the data at each common depth point (CDP), a correction was made for the moveout using velocities obtained from the velocity analysis.

Velocity Inversion

As described above, velocities were measured from the seismic data using a computerized inversion routine.

Muting

To remove refractions and other arrivals that were not completely removed using filtering techniques, we used trace muting before and after stacking.

Stacking

To enhance the seismic signal at each location, individual reflections were summed together in a process called stacking.

Depth Conversion

For stacked seismic reflection sections that were not migrated, we converted the time sections to depth sections using RMS velocities converted from the velocity analysis described above in the velocity section.

Migration

Due to the presence of faults and diffraction points in the subsurface, diffraction hyperbolae were observed throughout the section. We used pre-stack migration, a mathematical process that moves seismic energy (such as diffractions) back to there correct position in the subsurface, to collapse the diffraction hyperbolae.

Limitations of the Seismic Survey

The upper few feet of the subsurface along the Western Pacific Railroad consists of uncompacted-to-loose gravel. Shots fired into the subsurface along the railroad failed to propagate laterally for more than a few tens of meters, and most of those seismic signals propagated as fairly low-frequency (< 100 Hz) signals. The seismic survey was acquired in a highly urbanized area, with numerous industrial businesses. As a result, there was a high degree of cultural noise arising from generators, vehicles, hammers, etc. High levels of cultural noise usually do not present problems in high-resolution seismic imaging because the seismic signals are typically well above the frequency of the cultural noises, however, the cultural noises were problematic in this survey because the loose gravel of the Western Pacific Railroad prevented propagation of the higher frequencies. As a result of the low frequency seismic signals and the high levels of cultural noise, seismic refraction and reflection images of the subsurface were limited to about 40 m (~130 ft) and 150 m (~500 ft) depth, respectively.

Seismic Refraction Velocities

We inverted seismic refraction first-arrivals to generate a velocity model of the shallow subsurface (Fig. 7). Seismic velocities ranged from about 300 m/s in the uncompacted gravel to more than 3000 m/s at a depth of about 35 m. In general, the lower velocities extend to deeper depths on the NNE end of the seismic profile, with higher velocities nearer the surface toward the SSW end of the profile. Near the SSW end of the seismic profile (beyond meter 500), there is an abrupt rise in the higher velocity contours, suggesting a major change in structure. On the NNE end of the seismic profile, velocity contours dip sharply at depths below about 10 m, but it is possible that this sharp dip

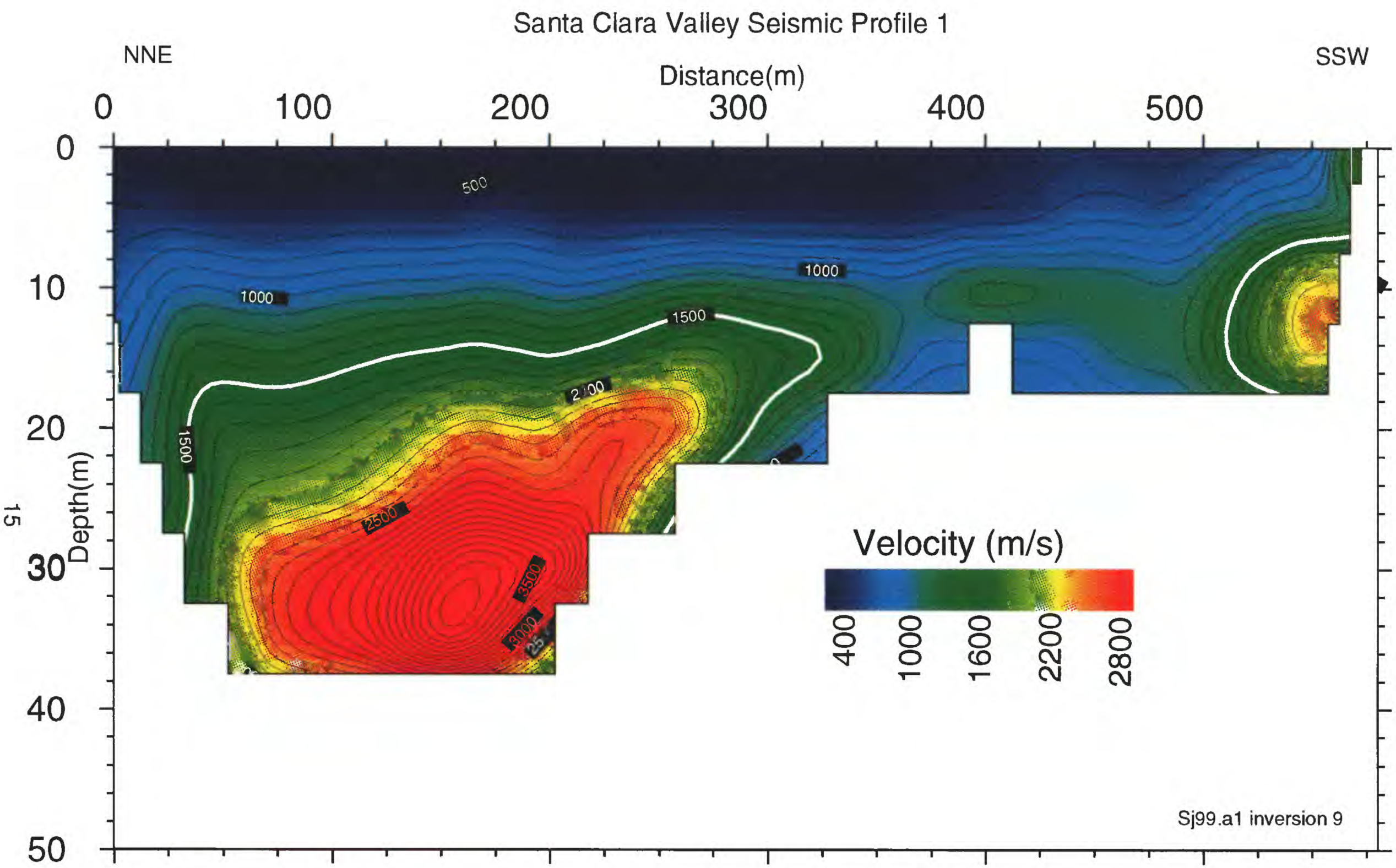

Fig. 7. Velocities measured along seismic profile 1 at depths less than 50 m (~ 164 ft). The white contour shows the lateral variation in the1500 m/s velocity, a velocity consistent with saturated sediments. Depth coverage is not uniform along the seismic profile because of variations in signal to noise ratios along the profile.

results from edge effects near the end of the profile. It is, however, unlikely that the dip on the SSW end of the profile results from edge effects because they occur at shallow depths where we have a high degree of data redundancy.

Velocities less than about 1500 m/s most likely represent unconsolidated sediments, but correlations between well-log data and similar seismic surveys elsewhere in California have shown that the 1500 m/s velocity contour corresponds to water-saturated, unconsolidated sediments (Catchings et al., 1998; Catchings et al., 1999b; Gandhok et al., 1999). Thus, along much of the velocity inversion model (Fig. 7), the 1500 m/s contour probably outlines the depth to water-saturated sediments. Velocities in excess of about 2500 m/s probably represent saturated clays or consolidated sediments.

Seismic Reflection Images

A migrated and interpreted seismic reflection image of the upper ~150 m is shown in figure 8. Color variations are used to highlight differences in the reflection character. The part of the image colored in yellow delineates a sequence of thin reflectors with close spacing between reflectors. These reflectors correspond to shallow sedimentary layers with velocities less than about 1000 m/s. The alternating brown and white coloration is used to help outline sequences of reflectors that have wider spacing between reflections, suggesting thicker layers. These layers probably represent sequences of clays and sands. Interpretable reflections occur above 50 m along the entire profile, but strong reflections are observed to approximately 150 m depth along the south-southwesternmost 200 m of the profile. It is unclear if these deeper (> 100 m) reflections are present between meters 0 and 400, but they are not as visible as those from meter 400 to meter 600. The lack of strong deep reflections between meters 200 and 400 may arise from higher cultural noises (industrial machinery) that masked our seismic signal in that distance range, or it may be due to subsurface structural changes (principally faulting) having displaced the layers more deeply to the north-northeast.

In the shallow section above about 20 m depth, individual reflectors can be traced across most of the profile, but these reflectors appear to be disrupted where the profile crosses streets. This disruption likely arises from either non-linearity of the geophone array where the array crossed the street (see figure 3) or to velocity variations associated with the paved streets. However, we can not rule out the possibility that the vertical offsets arise from faulting. In some locations, there are apparent offsets in layers that can not be attributable to geometrical variations in the geophone or shot arrays; these apparent offsets in reflectors probably represent faulting. Where there are apparently multiple layers with

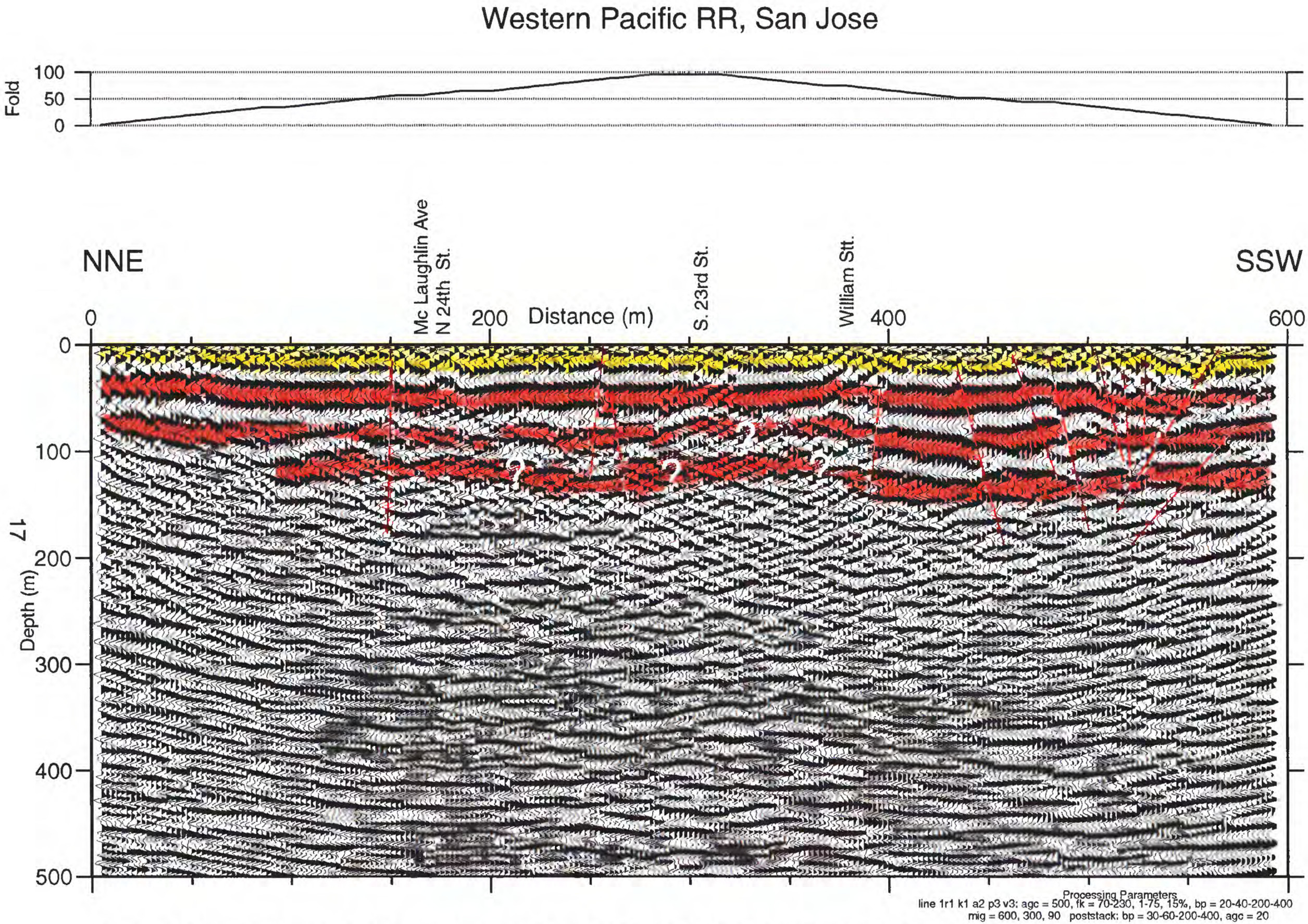

Fig. 8. Stacked, migrated, and interpreted seismic reflection image along profile 1. Yellow reflectors correspond to unconsolidated sediments with velocities less than about 2000 m/s. Brown and white reflectors suggest more consolidated sediments. Apparent offsets in layers (especially between meters 400 and 600) are interpreted as faulting (shown in red).

similar offsets, they have been marked with a red line to depict faulting. Small offsets are apparent at meters 175, 255, 400, however, the minor offset at meter 175 may be related to non-linearity of the seismic recording and shot arrays. A series of larger offsets are apparent between meters 400 and 600, which correlates with velocity variations observed on figure 6. For comparative purposes, an uninterpreted section is shown in figure 9.

Combined Velocity/Reflection Images

Due to the limited propagation distances along the Western Pacific railroad, seismic velocities are available to a shallow depth relative to depths afforded by the seismic reflection images (Fig. 10), but where we have both reflection and refraction images, the data show that the sequence of thin reflectors (described above in the seismic reflection section), correlates with velocities in the 300 m/s to 1400 m/s range (shown in blue). The thicker sequence of reflectors correlate with velocities ranging from about 1500 m/s (green) to over 3000 m/s (red). In general, velocities below the first strong reflection are in excess of 1500 m/s, suggesting that the reflection may correlate with the onset of water-saturated sediments.

Correlation with an INSAR Image

Possible faulting at meters 175 and 255 is apparent on both sides of the Silver Creek fault (as inferred from geologic mapping), but the sequence from meters 400-600 occur at the edge of the brightest part of the INSAR (Interferometric Synthetic Aperture Radar) image (Fig. 1), which infers the greatest uplift. Both the INSAR image and the velocity data are consistent with a suggests a shallower depth to saturated sediments to the southwest. In the velocity model, the 1500 m/s contour (velocity expected for saturated sediments) rises from NNE to SSW along most of the seismic profile but rises more abruptly toward the SSW end of the seismic profile. Considering the velocity data, the reflection image, and the INSAR image, we suggest that the eastern limit of the Silver Creek fault zone is probably located between meters 400 and 600, and it may be a water barrier.

Comparison to the Menlo Park Survey

An example of data acquired in a similar geological and environmental setting can be seen from an investigation (Catchings et al., 1998) at the Raychem site on Willow Road in Menlo Park, California (Fig. 11). The Raychem site consists of is underlain by similar

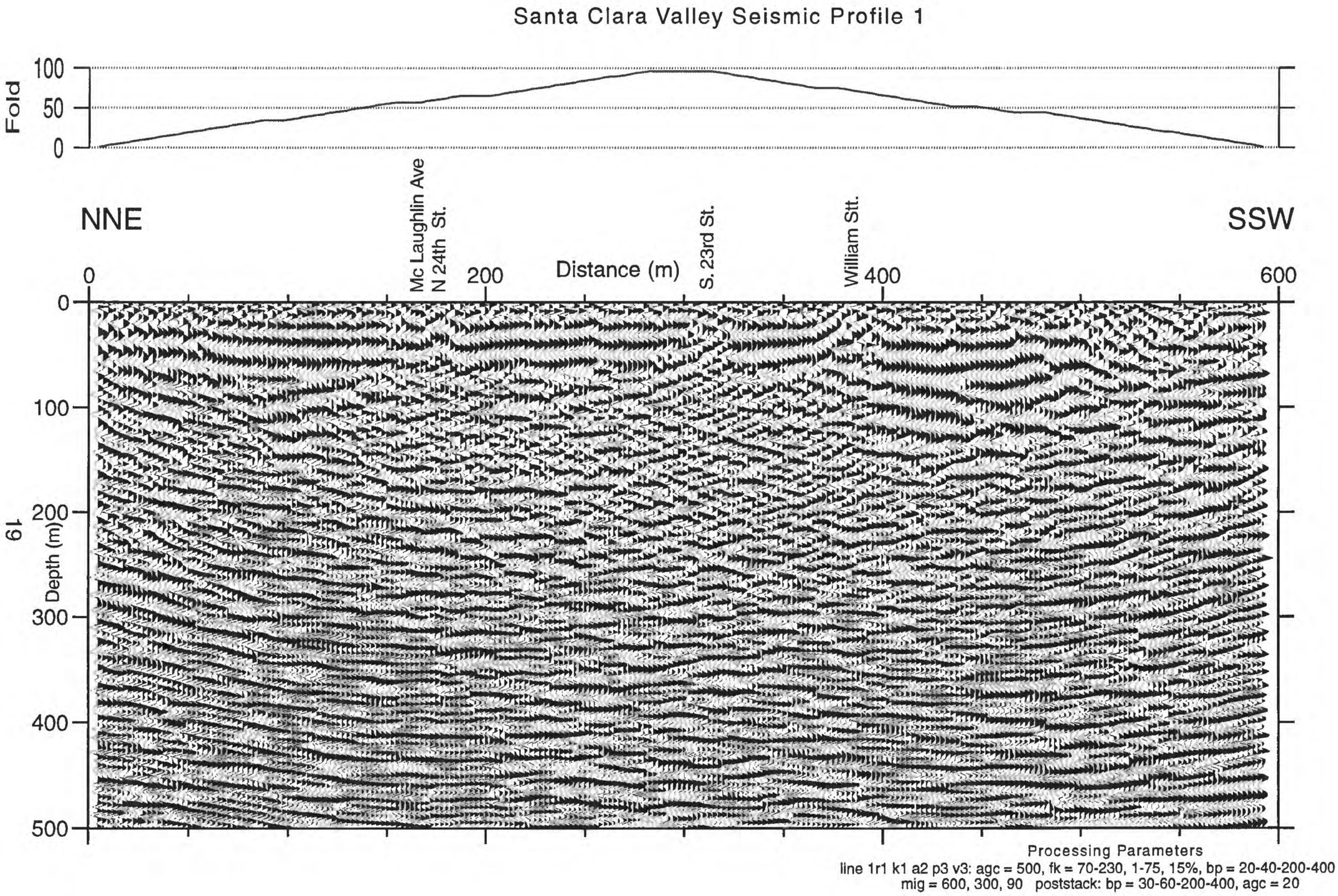

Fig. 9. Stacked and migrated seismic image of the upper 500 m along profile 1. Crossing streets are shown.

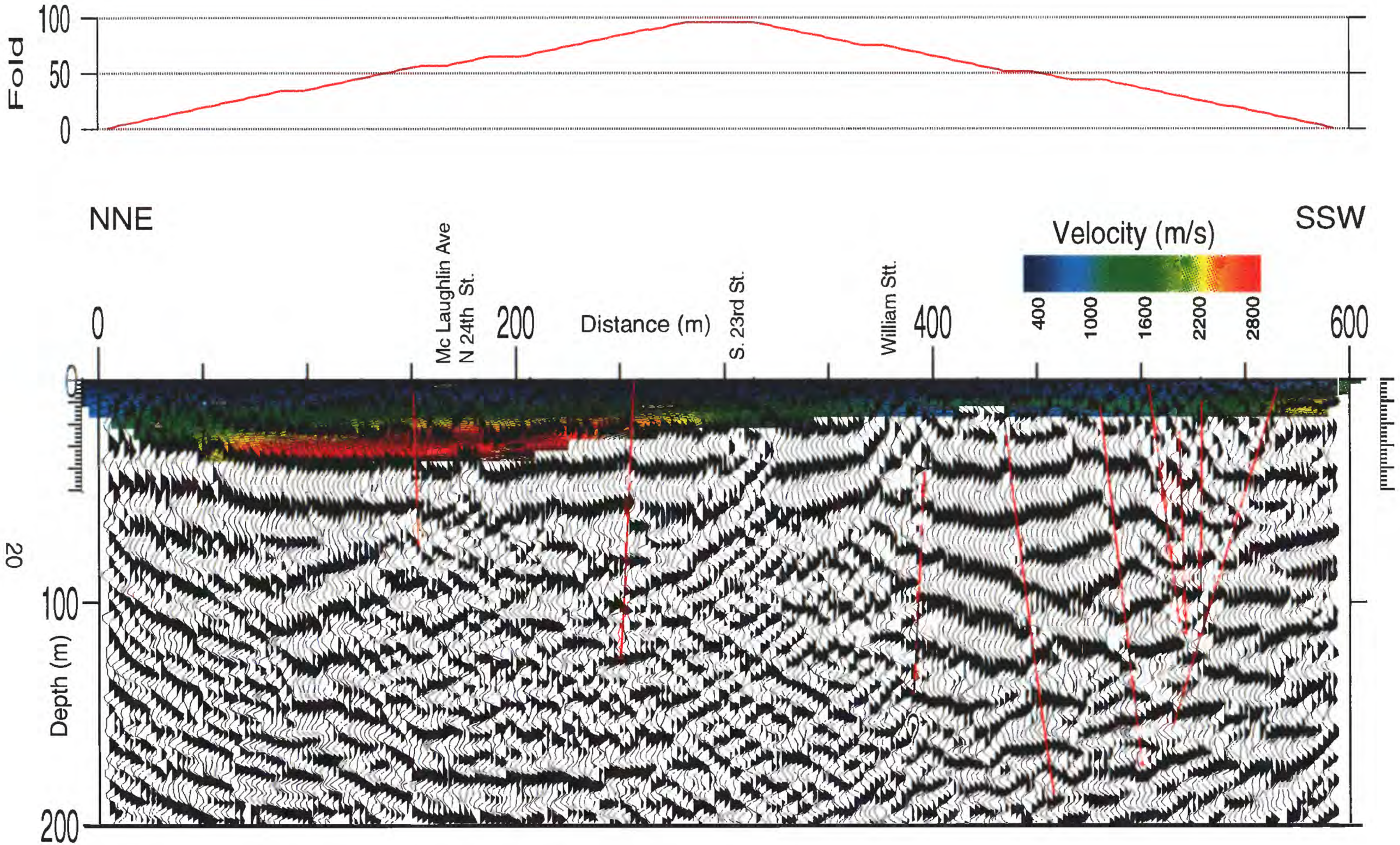

Fig. 10. Stacked, migrated, and interpreted seismic reflection image with velocity inversion model along the upper 200 m of profile 1. Interpreted faults are shown as red lines.

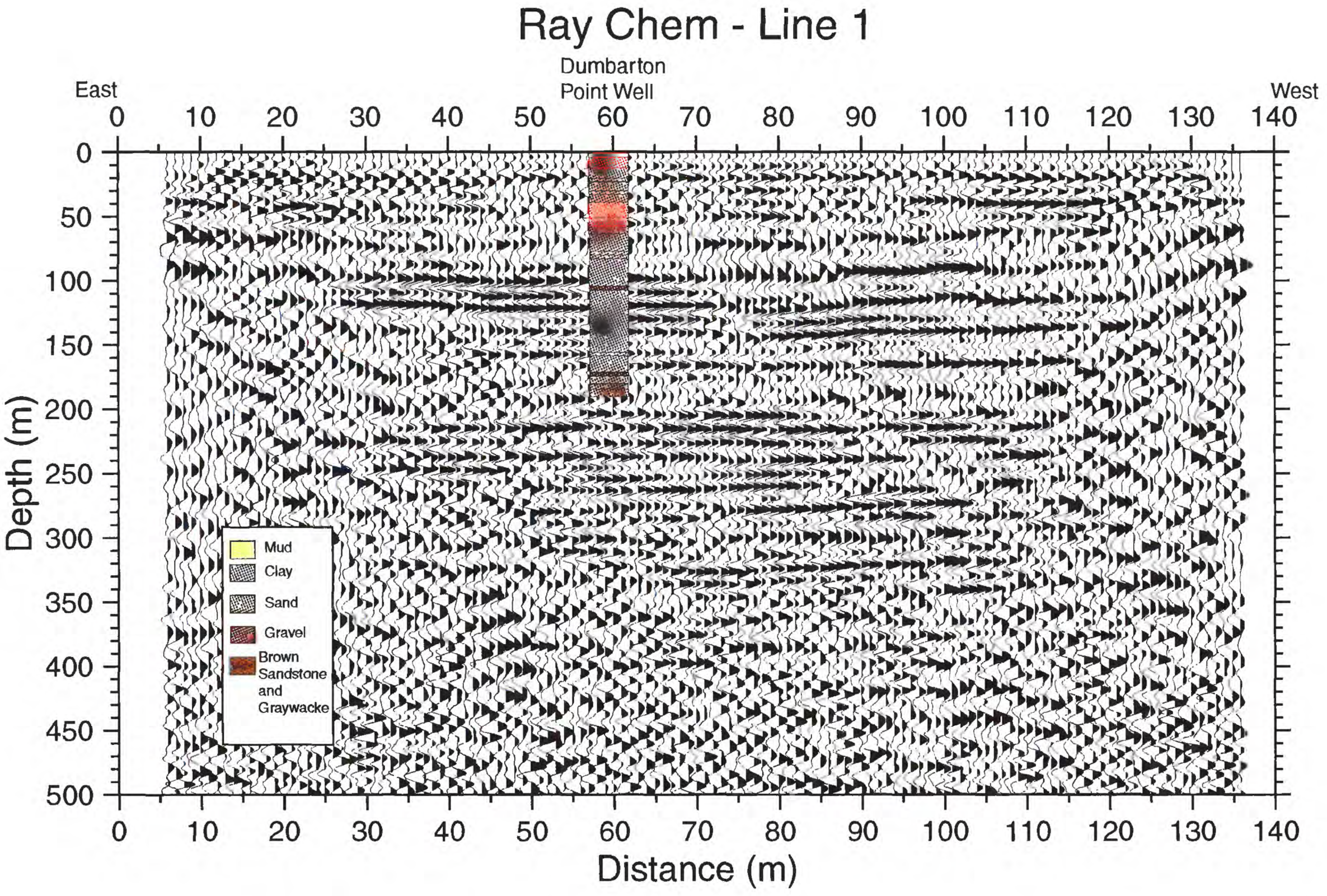

Fig. 11. Stacked seismic section of the upper 500 m beneath RC -1. The well log shown is from a well located about 1 km to the east of the Raychem site and described by Warrick (1974). Deeper seismic data are observed only in areas of high fold, near the center of the seismic array.

geological materials, principally sands, clays, and muds and near-surface gravel. However, the upper 0.5 m at the Raychem site consists of compacted gravels, which allow propagation of high-frequency seismic energy.

Comparison of the Santa Clara Valley (SCV) and the Raychem (RC) velocity models show similar velocities at similar depths (Fig. 12), suggesting similar geological materials beneath both sites. However, there are two principal differences in the overall velocity structure at the two sites: (1) Velocities of the near-surface gravels differ (due to the degree of compaction), and (2) the higher velocities (> 1600 m/s) at the SCV site are laterally discontinuous in the distance range between 300 and 500 m. The lower velocities are coincident with vertically offset reflectors observed in the reflection image (Fig. 8). As faulting is known to lower P-wave velocities, both measurements are consistent with faulting in the shallow subsurface there. Conversely, neither low velocities nor vertically offset layers are observed at the RC site(see Figs. 10 and 7).

Comparison of data from the two sites also demonstrates the attenuating effect of the uncompacted gravels on seismic signals. Cultural noise conditions at the RC site were similar or worse than those of the SCV site because the RC data were acquired within 10 m of a major traffic route during peak commuter periods and there were operating industrial machinery at the RC site. Furthermore, the RC data contained of much less fold (~60) in comparison to the SCV data (fold~95). Thus, one would expect poor signal quality and depth of propagation for the RC data. However, clear reflections representing depths of about 400 m were obtained at the RC site(Fig. 12), but reflections representing depths of only about 150 m were obtained at the SCV site (Fig. 8). The primary between difference between the seismic energy recorded at the two sites was the frequency content in comparison to that of the ambient noise. At SCV, the surficial gravel essentially filtered out the higher-frequency seismic signals such that they were largely comparable to the frequencies of the ambient noise. At the RC site, the compacted surficial materials allowed propagation of high-frequency seismic signals that were well above those of the ambient noise.

With high folds (>60) and the absence of surficial gravels, we suggest that seismic images to depths of about 500 m (~1600 ft) and velocity images to depths of about 150 m (~500 ft) are obtainable at most sites in the Santa Clara Valley when single-stack, seisgun sources are used. For greater depths, either multiple-stack, seisgun sources or small blasts are probably necessary.

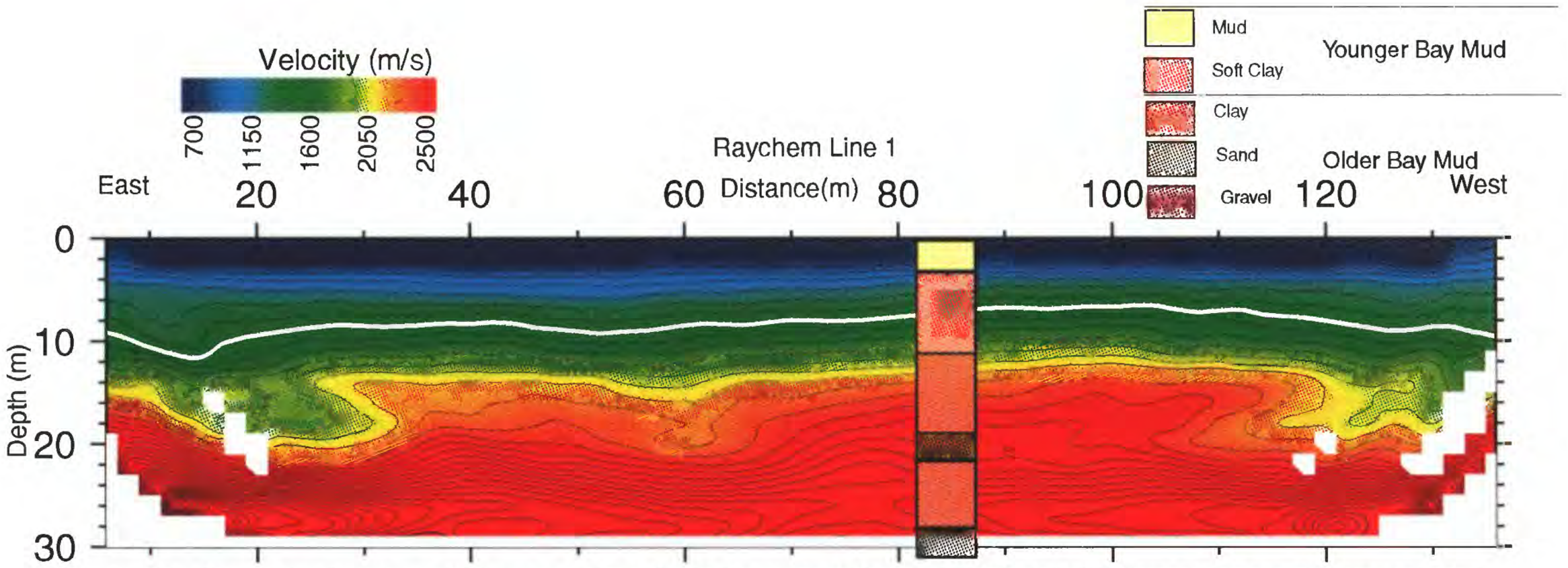

Fig. 12a. Seismic velocity inversion for the upper 30 m at the RayChem site. Velocities correlate well with differences among mud, clay, and sand. The well log and description shown are from a borehole approximately 1 km from the seismic profile (From Warrick,1974).

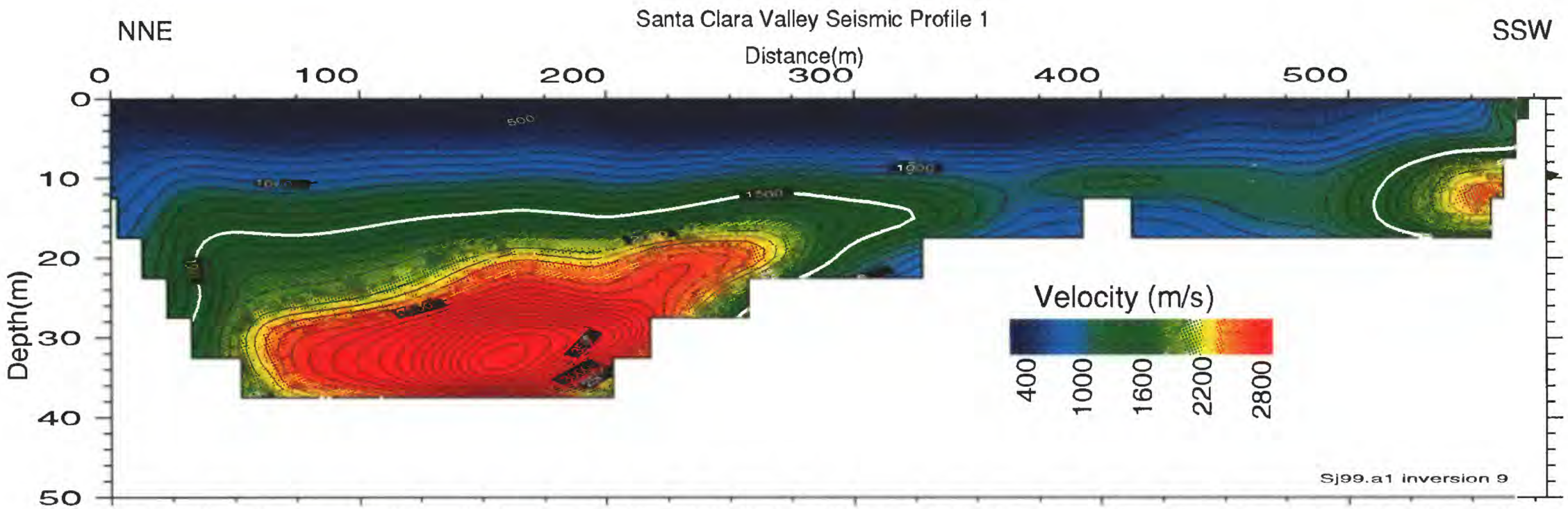

Fig. 12b. Velocities measured along SCV seismic profile 1 at depths less than 50 m (~ 164 ft). The white contours show the lateral variation in the 1500 m/s velocity, a velocity consistent with saturated sediments.

Summary

There were multiple objectives in conducting the seismic imaging test in the city of San Jose, including (1) a test of seismic acquisition parameters for the Santa Clara urban environment, (2) measurement of shallow subsurface velocities, (3) lateral mapping of subsurface stratigraphic units, and (4) imaging of possible faulting in the shallow subsurface. Most of the objectives of the seismic imaging test were realized.

The seismic imaging test suggests that high-resolution seismic imaging using Betsy Seisgun™ sources in the Santa Clara Valley is both possible and practical. In this particular test, loose gravels along the Western Pacific railway severely limited propagation of seismic energy, particularly high-frequency seismic energy, into the subsurface. Recorded frequencies were largely below about 100 Hz, and many were within the range of cultural noises in the valley. As a result, seismic reflection images were limited to about 100 m depth, and velocity images were limited to about 40 m depth. Future seismic investigations in the Santa Clara Valley should avoid profiling along railways if deeper imaging is desired. Comparable seismic imaging (with similar cultural noises) at about 30 km to the northwest in the Menlo Park area shows that reflections to depths in excess of about 400 m should be expected when the Betsy Seisgun ™ source is used in more consolidated materials. Thus, the results of this study suggest that high-resolution seismic imaging from depths of about 0.5 m (~1.75 ft) to about 500 m (~1600 ft) are obtainable within the Santa Clara Valley using single-stack Betsy Seisgun ™ sources. Velocity images to depths of about 150 m (~500 ft) are obtainable using the same sources and seismograph systems with favorable noise conditions. For greater depths, either multiple-stack Betsy Seisgun ™ sources or small blasts may be desirable.

The shallow-depth velocity structure is important for a number of reasons, including: (1) stacking seismic reflection data, (2) correlating reflection images with known stratigraphy, (3) mapping the water-saturated, unconsolidated sediments, and (4) modeling strong ground motions. In this study, we found that the seismic P-wave velocities in the upper 40 m beneath the Santa Clara Valley varied from about 500 m/s near the surface to about 3500 m/s at a depth of about 40 m. At both the San Jose and the Raychem sites, P-wave velocities of in excess of 2000 m/s are observed at depths of about 20 m, suggesting predominantly clay layers at those depths.

The seismic data, both reflection images and velocity images, suggest lateral variation in the subsurface stratigraphic layers. The possible clay layers may have been laterally disrupted (probably faulted) at the SCV site near the suspected location of the Silver Creek fault. Velocities (>1500 m/s) consistent with water-saturated sediments are

observed within the upper 6 meters on the SSW end of the SCV profile, but similar velocities are observed at about 10-14 m depth on the NNE end of the profile. These observations are consistent with the INSAR image (Fig 1b), which may indicate lower water depths on the NNE end of the seismic profile across the Silver Creek fault.

The stacked and migrated seismic reflection images at the SCV site suggest that the most pronounced offsets of stratigraphic layers occur between meters 400 and 600 of the seismic profile (Fig. 8), which is approximately the location of the brightest part of the INSAR image (Fig. 1b). Near about 400 meter, reflections at 100 m depth are less clear, but we do not know if the loss in reflection strength is due to stratigraphic changes or to a lack of signal strength. If the loss in reflection strength is due to stratigraphic changes, then the area near meter 400 may be a principal fault associated with the Silver Creek fault. The offset reflections between meter 400 and 600, combined with the change in velocity structure in that area, suggest that there is a zone of faulting that reaches the near surface in that area. The possible fault at meter 400 and the faulting between meters 400 and 600 together, probably constitute the Silver Creek fault zone, which is at least 100 to 200 m wide. Disturbances in layering within the upper 5 m of the surface suggests that these probable faults can be trenched for accurate dating of their most recent movement. If the Silver Creek fault zone extends nearly 70 km, as inferred from geologic mapping, and if it is still active, it may pose as great or greater seismic hazard to the Santa Clara Valley than do the Hayward and Calaveras faults.

Numerous studies have shown that faulting in sediments may contribute to segmentation of the groundwater flow patterns. The vertical offsets suggested by the seismic data in this study may disrupt the lateral continuity of the aquifer system. Identification of the faulting patterns and their effect on the groundwater flow system throughout the Santa Clara Valley may be possible with strategically placed high-resolution seismic imaging studies.

Acknowledgments

We thank Devin Galloway and Peter Martin for suggesting the seismic test and for providing the INSAR data. Funding was provided by the Santa Clara Valley Water District, the US Geological Survey Water Resources Division, and the US Geological Survey Western Earthquake Hazards Team. We thank the Western Pacific Railroad for access and Randy Hansen for negotiations with the Western Pacific Railroad. We thank Joe Catchings, Jeff Dingler, Andy Gallardo, Samantha Hansen, Keith Rice, and Chizuru Suzuki for field assistance, and we thank John Hamilton for surveying the shots and recording sites.

References

Bortugno, E.J., R.D. McJunkin, and D.L. Wagner, 1991, Map showing recency of faulting, San Francisco-San Jose Quadrangle, California, 1:250,000.

Catchings, R. D., E. Horta, M. R. Goldman, M. J. Rymer, and T. R. Burdette, 1998, High-Resolution Seismic Imaging For Environmental and Earthquake Hazards Assessment at the Raychem Site, Menlo Park, California, US Geological Survey Open-file Report 98-146, 37 pp.

Catchings, R. D., M. R. Goldman, G. Gandhok, E. Horta, M. J. Rymer, P. Martin, and A. Christensen, 1999, Structure, Velocities, and Faulting Relationships Beneath San Gorgonio Pass, California: Implications for Water Resources and Earthquake Hazards, US Geological Survey Open-file Report 99-568, 53 pp.

Gandhok, G., R. D. Catchings, M. R. Goldman, E. Horta, M. J. Rymer, P. Martin, and A. Christensen, 1999, High-Resolution Seismic Reflection/Refraction Imaging from Interstate 10 to Cherry Valley Boulevard, Cherry Valley, Riverside County, California: Implications for Water Resources and Earthquake Hazards, US Geological Survey Open-file Report 99-320, 52 pp.

Hole, J. A., 1992, Nonlinear high-resolution three-dimensional seismic traveltime tomography, Journal of Geophysical Research, v. 97, p. 6553-6562.

Schon, J. H., 1996, Physical Properties of Rocks: Fundamentals and Principals of Petrophysics, Handbook of Geophysical Exploration, Seismic Exploration Vol 18, Elsevier Science, Inc., Tarrytown, N. Y.

Wagner, D.L., E.J. Bortugno, and R.D. McJunkin, 1991, Geologic Map of the San Francisco-San Jose Quadrangle, 1:250,000.

Warrick, R.E., 1974, Seismic investigation of a San Francisco Bay mud site, Bull. Seismol. Soc. Am, v. 64, pp. 375-385.

Wentworth, C.M., M.C. Blake, Jr., R.J. McLaughlin, and R.W.Graymer, 1999, Preliminary geologic description of the San Jose 30 x 60 minute quadrangle, California, Part 3 of US Geological Survey Open-File Report 98-795, 52pp.

		Appendix A			
Shot #	Shot Dist. (m)	Elevation (m)	Geo. #	Geo Dist. (m)	Elevation (m)
1	0	0.14			
2	4.81	0.14			
3	9.88	0	3	9.9	0.3
4	14.66	0.12	4	14.68	0.31
5	20.04	0.13	5	19.89	0.32
6	25.05	0.13	6	25.09	0.25
7	29.88	0.06	7	29.94	0.26
8	34.81	0.08	8	34.61	0.31
9	39.81	0.16	9	39.81	0.28
10	44.8	0.22	10	44.7	0.33
11	49.8	0.24	11	49.71	0.37
12	54.84	0.19	12	54.65	0.3
13	59.71	0.19	13	59.64	0.26
14	64.72	0.13	14	64.65	0.23
15	69.68	0.16	15	69.64	0.24
16	74.83	0.13	16	74.81	0.16
17	79.88	0.13	17	79.81	0.18
18	84.99	0.17	18	84.98	0.17
19	89.77	0.12	19	89.7	0.16
20	94.77	0.18	20	94.69	0.16
21	99.91	0.11	21	100	0.12
22	104.67	0.16	22	104.73	0.17
23	109.74	0.21	23	109.81	0.2
24	114.91	0.19	24	114.89	0.21
25	119.83	0.21	25	119.8	0.25
26	124.77	0.25	26	124.89	0.25
27	129.9	0.24	27	129.85	0.28
28	134.98	0.33	28	134.85	0.36
29	139.89	0.36	29	139.8	0.42
30	144.77	0.44	30	144.7	0.52
31	149.88	0.45	31	149.8	0.56
32	154.75	0.46	32	154.9	0.64
33	159.83	0.54	33	160.17	0.72
34	164.65	0.66	34	164.52	0.78
39	190.04	0.55	35	168.43	0.75
40	194.85	0.62	36	174.11	0.75
41	199.64	0.59	37	179.28	0.79
42	204.8	0.66	38	184.45	0.8
43	209.52	0.55	39	190.14	0.58
44	214.67	0.62	40	194.9	0.68
45	219.6	0.64	41	199.7	0.59
46	224.75	0.66	42	204.67	0.66
47	229.62	0.71	43	209.58	0.66

48	234.67	0.73	44	214.6	0.72
49	239.64	0.75	45	219.59	0.72
50	244.53	0.85	46	224.76	0.73
51	249.56	0.88	47	229.66	0.76
52	254.63	0.84	48	234.63	0.77
53	259.84	0.81	49	239.73	0.78
54	264.74	0.76	50	244.6	0.91
55	269.64	0.68	51	249.69	0.94
56	274.59	0.72	52	254.58	0.87
57	279.95	0.77	53	259.91	0.86
58	284.87	0.73	54	264.74	0.85
59	289.75	0.79	55	269.75	0.78
60	294.76	1.05	56	274.64	0.78
61	299.85	1.06	57	279.65	0.8
67	329.65	0.87	58	284.79	0.77
68	334.73	0.83	59	289.82	0.87
69	339.73	0.8	60	294.7	1.09
70	344.7	0.89	61	299.97	1.08
71	349.62	0.9	62	304.84	0.96
72	354.68	0.98	63	309.45	1.07
73	359.74	1.02	64	314.37	1.07
74	364.41	1.02	65	319.67	1
81	399.47	0.89	66	324.56	0.7
82	405.16	0.85	67	329.79	0.83
83	409.9	0.76	68	334.7	0.84
84	414.6	0.67	69	339.77	0.84
85	419.6	0.74	70	344.66	0.89
86	424.51	0.72	71	349.59	0.85
87	429.66	0.67	72	354.58	0.9
88	434.54	0.63	73	359.61	1.01
89	439.55	0.63	74	364.5	1.14
90	444.36	0.6	75	369.32	1.18
91	449.43	0.63	76	374.34	1
92	454.57	0.57	77	379.37	1
93	459.65	0.57	78	384.4	1
94	464.43	0.48	79	389.42	1
95	469.49	0.49	80	394.45	1.04
96	474.31	0.4	81	399.48	0.82
97	479.56	0.44	82	404.89	0.78
98	484.49	0.49	83	409.59	0.77
99	489.46	0.54	84	414.36	0.73
100	494.59	0.46	85	419.73	0.74
101	499.45	0.48	86	424.45	0.72
102	504.56	0.48	87	429.6	0.76
103	509.62	0.47	88	434.58	0.64
104	514.61	0.47	89	439.49	0.67

106	524.16	0.38	90	444.37	0.65
107	529.41	0.4	91	449.33	0.67
108	534.29	0.39	92	454.63	0.59
109	539.11	0.33	93	459.72	0.58
110	544.36	0.35	94	464.6	0.58
111	549.38	0.27	95	469.59	0.54
112	554.55	0.28	96	474.35	0.52
113	559.51	0.23	97	479.56	0.52
114	564.59	0.23	98	484.57	0.5
115	569.26	0.16	99	489.37	0.56
116	574.48	0.21	100	494.48	0.51
117	579.5	0.17	101	499.51	0.51
118	584.61	0.14	102	504.21	0.44
119	589.43	0.1	103	509.34	0.45
120	594.55	0.13	104	514.53	0.44
121	599.59	0.13	105	519.43	0.48
122	604.44	0.13	106	524.49	0.42
123	609.56	0.09	107	529.4	0.45
124	614.59	0.06	108	534.35	0.38
125	619.6	0.04	109	539.42	0.36
			110	544.36	0.33
			111	549.68	0.31
			112	554.66	0.25
			113	559.61	0.26
			114	564.5	0.28